Available online at www.sciencedirect.com
ScienceDirect
Journal of the European Ceramic Society 29 (2009) 2893–2901
www.elsevier.com/locate/jeurceramsoc

Densification, microstructure and mechanical properties of ZrB_2–SiCw ceramic composites

Tao Zhu [a], Lin Xu [a,*], Xinghong Zhang [a], Wenbo Han [a], Ping Hu [a], Ling Weng [a,b]

[a] *Center for Composite Materials, Harbin Institute of Technology, Harbin 150001, PR China*
[b] *The school of Material Science & Engineering, Harbin University of Science and Technology, Harbin 150040, PR China*

Received 25 November 2008; received in revised form 26 February 2009; accepted 16 March 2009
Available online 18 April 2009

Abstract

ZrB_2–SiCw composites were prepared through hot-pressing at a low temperature of 1800 °C, and Al_2O_3 plus Y_2O_3 were added as sintering aids. Analysis revealed that additives may react with impurities (i.e. surface oxygen impurities and residual metallic impurities) to form a transient liquid phase, thus promote the sintering and densification of ZrB_2–SiCw composites. The content of additives was found to have a significant influence on the sinterability, microstructure and mechanical properties of ZrB_2–SiCw composites. ZrB_2–SiCw composite prepared with a small amount of additives (3 vol.%) provided the optimal combination of microstructure (relative density of 98.3%) and excellent properties, including flexural strength of 783 MPa and fracture toughness of 6.7 MPa $m^{1/2}$. With further addition of additives, SiC whiskers were inclined to gather together and be enveloped by excessive liquids to form core-rim-like structures, which lead to little decrease in mechanical properties.

Keywords: ZrB_2; SiC whisker; Sinterability; Microstructure; Mechanical property

1. Introduction

IV–V-group transition metal diborides and carbides are thought to be the potential candidates for use at very high temperature (>2200 °C) due to their high melting points, i.e. above 3000 °C.[1] For instance, as representatives of so-called ultra-high temperature ceramics (UHTCs), zirconium diborides (ZrB_2) and hafnium diboride (HfB_2) possess melting temperatures of 3247 and 3380 °C, respectively.[2] These refractory metal diborides were historically studied and developed since the late 1960s and early 1970s.[3,4] In recent years, they have attracted researchers from different fields and many experimental[5–14] as well as theoretical studies[15–18] are going on in these materials.

Among MB_2-typed (M = Zr or Hf) matrix ceramic composites, ZrB_2–SiC and HfB_2–SiC are reported to have good combination of mechanical properties, high temperature ablation/oxidation and thermal shock resistance.[2–7] These peculiarities make them attractive candidates for high temperature applications such as refractory in foundries, electrical devices, nozzle or armour and high temperature structural applications in aerospace.

Compared to its potential, the applications of MB_2 are rather limited, mainly because of the difficulties that exist in obtaining fully dense materials. Besides strong covalent bond, low diffusion coefficient and presence of oxide layers (i.e. B_2O_3, ZrO_2, and HfO_2) pose additional detrimental effects on the consolidation of composites.[5,19] Therefore, MB_2 ceramics have only been densified by hot-pressing at a temperature of 2000 °C or above with moderate pressure (~30 MPa),[2,20] or lower temperature (~1800 °C) with much higher pressure (>800 MPa).[21,22] In order to improve the sinterability of MB_2, metallic additions such as Ni,[23] Cu,[24] Fe[25] and Cr[25] have been used as sintering aids. However, the adoption of metals generally degrades both room temperature and high temperature properties of composites, due to the introduction of low melting point residual secondary phases. Recently, a group of ceramic-like additives including $MoSi_2$,[26] AlN,[27] Si_3N_4,[19] $ZrSi_2$,[28] Y_2O_3,[29] BC_4[30]and C[31] were successfully employed to improve the sinterability of MB_2, attributing to the introduction of a liquid phase or removal of surface oxides. Particularly, combination of Si_3N_4, Al_2O_3 and Y_2O_3 enables ZrB_2–SiC composite to be fully densified at a relative low temperature of 1760 °C.[19] Unfortunately,

* Corresponding author. Tel.: +86 451 86402382; fax: +86 451 86402382.
E-mail address: xulinhit@yahoo.com.cn (L. Xu).

0955-2219/$ – see front matter © 2009 Elsevier Ltd. All rights reserved.
doi:10.1016/j.jeurceramsoc.2009.03.008

the role of additives especially Al_2O_3 and Y_2O_3 as well as their contents on microstructure and mechanical properties are not well known.

In the present study, the ZrB_2-based composites reinforced by SiC whiskers were hot-pressed at 1800 °C with the addition of Al_2O_3 and Y_2O_3 as sintering aids. The solidification mechanism and function of additives were investigated. The effect of additives content on densification behavior, microstructure and mechanical properties were also examined and discussed. Due to their high cost, HfB_2-based compositions were not included in this study.

2. Experimental procedure

2.1. Materials preparation

Commercially available raw materials were used in this study. The ZrB_2 powder with a mean size of 2–3 μm (purity 99%) was supplied from Northwest Institute for Non-ferrous Metal research, China and β-SiC whisker from Alfa Aesar, MA, USA (purity 99%). The whisker used here has a diameter of 0.2–1.0 μm and a length of 10–50 μm. The Al_2O_3 and Y_2O_3 powders (average grain size 1 μm, purity 99%) from Sanxin Co. Ltd., Shanghai, China were used as sintering additives. Four groups of powder mixtures were designed as shown in Table 1. Hereafter, according to the content of sintering aids, the composites are referred to as ZW, ZW3AY, ZW6AY and ZW10AY, respectively.

Before mixing, the SiC whiskers were firstly dispersed by ultrasonication and a mechanical homogenization for 1 h. And then, the dispersed SiC whiskers with ZrB_2 powders, Al_2O_3 and Y_2O_3 sintering additives were ball-milled for 10 h in a polyethylene bottle using ZrO_2 balls and ethanol as the grinding media. It should be noted that the attrition milling speed must be restricted in 200 rpm for protecting SiC whiskers from damage. After mixing, the solvent was removed by rotary evaporation to minimize segregation during drying due to differences in the sedimentation rates of different powders. The resulting powder mixtures were hot-pressed at 1800 °C for 60 min under a uniaxial load of 30 MPa in Argon atmosphere in BN-lined graphite dies. In order to reduce the influence of sintering parameters on the densification and microstructure, composite without additives (ZW) was also prepared under the same condition for comparison.

Table 1
Materials design, composition and their corresponding density after hot-pressing (bulk density Bd, relative density Rd).

Materials	Compositions (vol.%)			Density	
	ZrB_2	SiCw	$(Al_2O_3 + Y_2O_3)$[a]	Bd (g cm^{-3})	Rd (%)
ZW	80	20	0	5.24	95.0
ZW3AY	77	20	3	5.37	98.3
ZW6AY	74	20	6	5.30	97.8
ZW10AY	70	20	10	5.22	97.5

[a] The molar ratio of Al_2O_3 andY_2O_3 was kept at 5:3.

2.2. Characterization

After densification, bulk density of hot pressed billet was determined using the Archimedes' method, while the relative density was estimated by the ratio of bulk value to theoretical value which was calculated by the rule of mixture. All samples were smoothly polished using a diamond paste and ultrasonic cleaned. Phase composition was determined via X-ray diffraction using Cu Kα radiation. The microstructure features and fragmented surfaces of the composite were observed by scanning electron microscopy (SEM) with simultaneous chemical analysis by energy dispersive spectroscopy (EDS). Characterization of the microstructure especially the interface of composites was also performed by transmission electron microscopy (TEM) and high-resolution electron microscopy (HREM). Thin foils of samples were prepared by grinding, dimpling and subsequent ion-beam thinning.

Flexural strength (σ) was tested in three-point bending on 4 mm by 3 mm by 36 mm (width by height by length) bars, using a 30 mm span and a crosshead speed of 0.5 mm min^{-1}. Each specimen was ground and polished with diamond slurries down to a 1 μm finish. The edges of all the specimens were chamfered to minimize the effect of stress concentration due to machining flaws. Fracture toughness (K_{IC}) was evaluated by a single-edge notched beam test with a 16 mm span using 2 mm by 4 mm by 22 mm (width by height by length) test bars, on the same jig used for the flexural strength. All flexural bars were fabricated with the tensile surface perpendicular to the hot-pressing direction. A minimum number of five specimens were tested for each experimental condition.

3. Results and discussion

3.1. Densification mechanism

The shrinkage curves collected during hot-pressing are plotted in Fig. 1 as a function of the sintering time, along with the temperature profile. The ZW3AY composite started to shrink at about 1650 °C and the overall duration of the thermal treatment

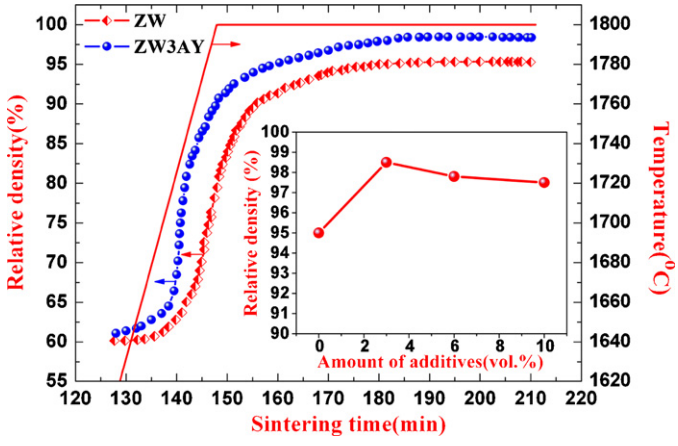

Fig. 1. Relative density (left *Y*-axis) in function of sintering time for ZW and ZW3AY. Solid line describes the temperature schedule (right *Y*-axis). Inset: relative density as a function of additive content.

was about 210 min. However, ZW sample (with no additives) began to have a measurable shrinkage at around 1720 °C. After densification, the relative density of ZW was only 95% of the theoretical density. It increased to 98.3% when 3 vol.% sintering additives was adopted even hot-pressed under the same conditions. These differences should be attributed to the introduction of sintering additives. Al_2O_3 and Y_2O_3 favor to form a liquid phase, namely $Y_3Al_5O_{12}$ (YAG), with the molar ratio of 5:3 at relative low temperature.[32,33]

Fig. 2 shows a TEM image of a specimen from ZW3AY with the corresponding selected area electron diffraction (SAED). EDS spectrum (same to Fig. 4b and d) and SAED image revealed the surrounding grains (marked as "z") were ZrB_2, with $c/a \approx 1.11$ as the lattice parameter ratio, and the triple pocket phase was rich in O, Al and Y, which was labeled as "p". It was noted that B, Si, Zr and Mg were also found in this "p" phase. This suggests that B_2O_3, SiO_2, ZrO_2, being the surface oxide impurities of starting powders,[19,30] and little metallic impurity (i.e. Mg) react or dissolve with/into Al_2O_3 and Y_2O_3 under the sintering condition. Such behaviors may lower the melting point of the liquid phase and in turn promote the densification of ZrB_2–SiCw composite. The ring diffraction patterns in Fig. 2 further indicates that this phase is polycrystal structure with nano-size. It was formed by cooling and recrystallizing from liquid state at high temperature to crystal phase at room temperature. Moreover, this transient liquid medium is known to drive the activity, diffusion rate of the atomic species and rearrangement of grain organization involved in the densification mechanisms, which help the powders compact to densify earlier and faster (Fig. 1).[32,33]

The relative density of four composites is presented in Fig. 1 (see inset). Inspection of this figure suggests that all three composites with sintering aids have higher relative density than ZW. This indicates Al_2O_3 and Y_2O_3 bring beneficial effect to the densification of ZrB_2–SiCw. Meanwhile, with increase in additive content, the densification of hot-pressed ceramics shows evident enhancement from 95% for ZW to 98.3% for ZW3AY, and then no obvious increment with further addition. In the later section, the effect of additives on the relative density will be analyzed in more details.

3.2. Microstructure

Fig. 3 shows SEM micrographs of polished surfaces of the ZrB_2–SiCw composites with different content of sintering additives. Together with the high-magnification SEM image of ZW3AY in Fig. 4, EDS patterns reveal that the microstructure is characterized by the presence of gray ZrB_2 matrix, as well as dark acicular-like SiC whiskers. Some pores are distinguished in ZrB_2–SiC composite without sintering additives (ZW), especially in the conjoint points of the ZrB_2 grains and SiC whiskers as shown in Fig. 3a. This is consistent with the relative low density of the corresponding composite (Fig. 1). Comparing the SEM photographs shown in Fig. 3b–d, it is seen that microstructure changes very little with the increasing content of additives under this magnification.

In order to study the effect of sintering additives on the microstructure of ZrB_2–SiCw composites, specimens with the surface parallel to the hot-pressing direction were prepared through cutting, grinding and polishing. And then, these specimens were analyzed using SEM. Figs. 4 and 5 show the high-magnification SEM images and the corresponding EDS results of ZrB_2–SiCw composites with different content of additives. As illustrated in Fig. 4, besides ZrB_2 and SiC whiskers, small amount of O–Al–Y rich glass phase was detected to be located at the conterminous section of ZrB_2 grains and SiC

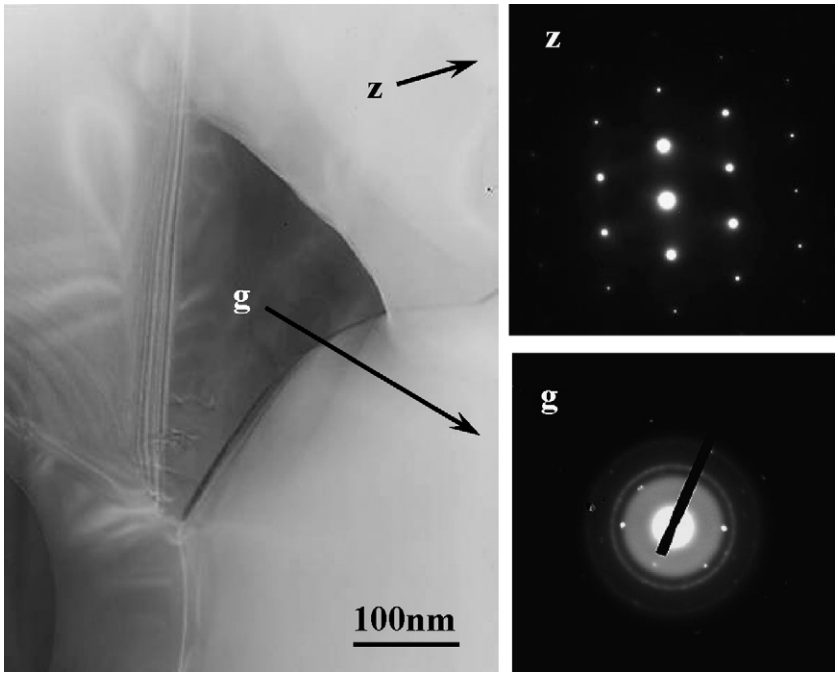

Fig. 2. TEM micrograph of a triple pocket phase in sintered ZW3AY composite, also given their corresponding SAED images.

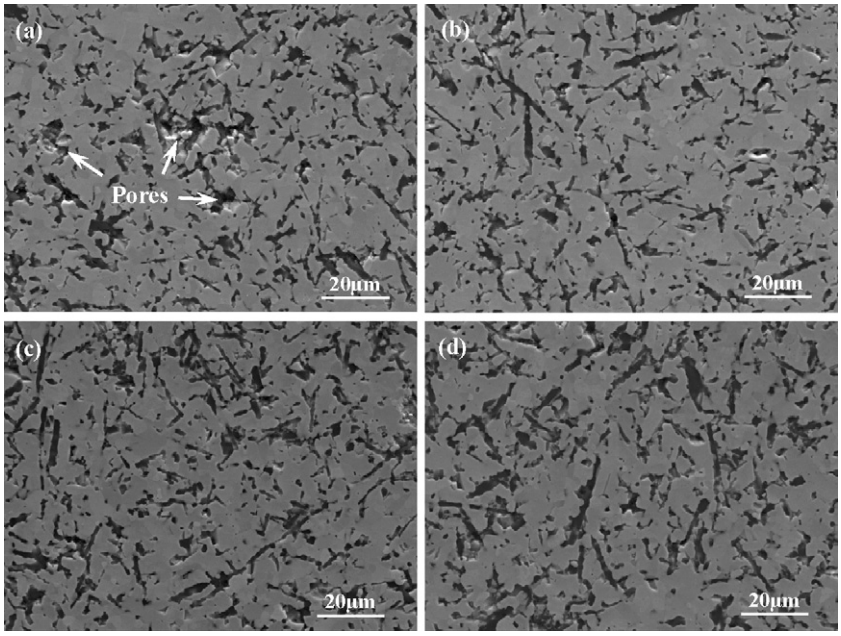

Fig. 3. SEM micrograph of polished surface of ZrB_2–SiCw composites with different additives contents: (a) 0, (b) 3, (c) 6, and (d) 10 vol.%.

whiskers. This is referred to the transient liquid phase as mentioned previously.

High-magnification SEM photographs of ZW6AY is shown in Fig. 5. The polished surface was investigated through doing line scan analyses by energy dispersive spectroscopy, and the variations in Zr, Si, O, Al, Y concentrations are also plotted in Fig. 5. It is interesting to note that the microstructure showed a core-rim-like structure of SiC whiskers, which is different from the ZrB_2–SiCw composite with small amount of additives (3 vol.%) as shown in Fig. 4. Extensive EDS linescans analyses reveal this core-rim-like structure consists of an inner SiC whiskers core surrounded and filled by additive glass phase with in rich O, Al and Y. The microstructure of ZW10AY was the same as that of ZW6AY except more amount of glass phase in the core-rim alike structure.

Figs. 6 and 7 are TEM analyses and schematic illustration of the sintered ZrB_2–SiCw composites with different amount of additives. The overall characteristic of the microstructures can be observed, which basically coincides with that of scanning electron microscopy analyses results. Although a number of excellent research works have been reported on the sintering of non-oxide ceramics, the mechanisms of sintering activation

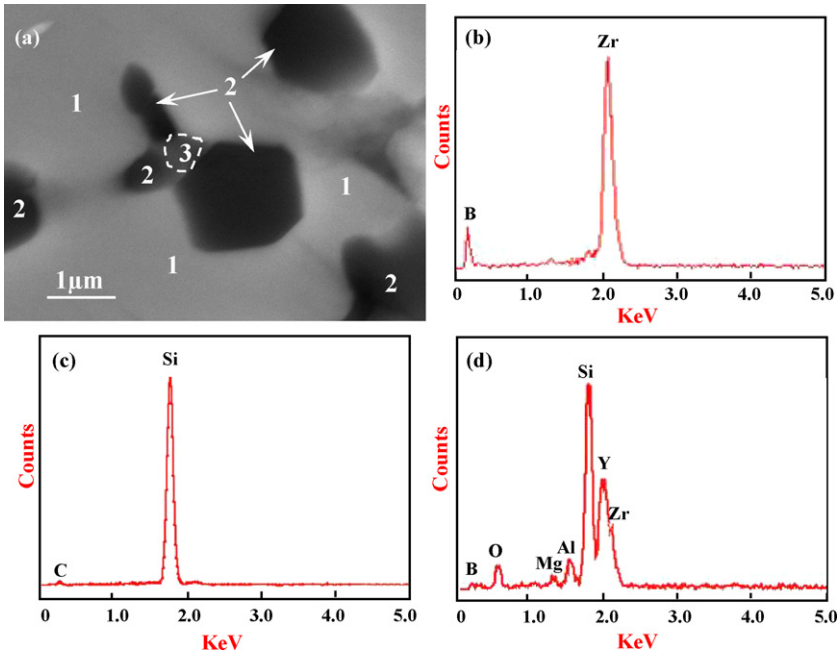

Fig. 4. High-magnification SEM micrograph of polished surface from ZW3AY (a). EDS analyses correspond to the numbered regions, as follows: 1 → ZrB_2 (b), 2 → SiC (c), 3 → O–Al–Y–B–Si–Zr–Mg (d).

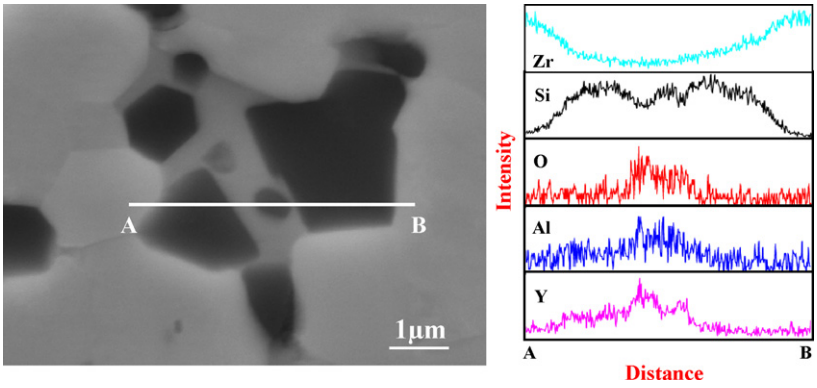

Fig. 5. High-magnification SEM micrograph of polished surface from ZW6AY (a). EDS linescans showing the variation in Zr, Si, O, Al and Y concentrations across ZrB_2 grains and SiC whiskers indicated in the SEM image.

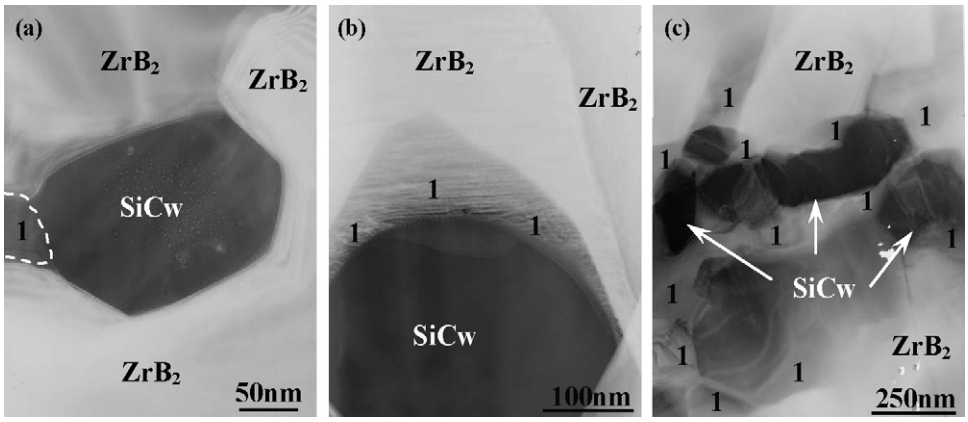

Fig. 6. TEM micrographs of ZrB_2–SiCw composite with different amount of additives: (a) 3, (b) 6, and (c) 10 vol.%. "1" represents additives.

by means of doping with sintering additives is still a much-discussed topic. Through the final microstructure configuration in Figs. 2–7, the role of liquid-formation additives during sintering in the present study can be explained as follows.

As with other non-oxide ceramics, ZrB_2 exhibits strong covalent bonding and low grain boundary diffusion coefficients.[5] It is also known that oxygen contamination on the surface of raw powders (i.e. ZrB_2, SiC whiskers) will retard the diffusion mech-

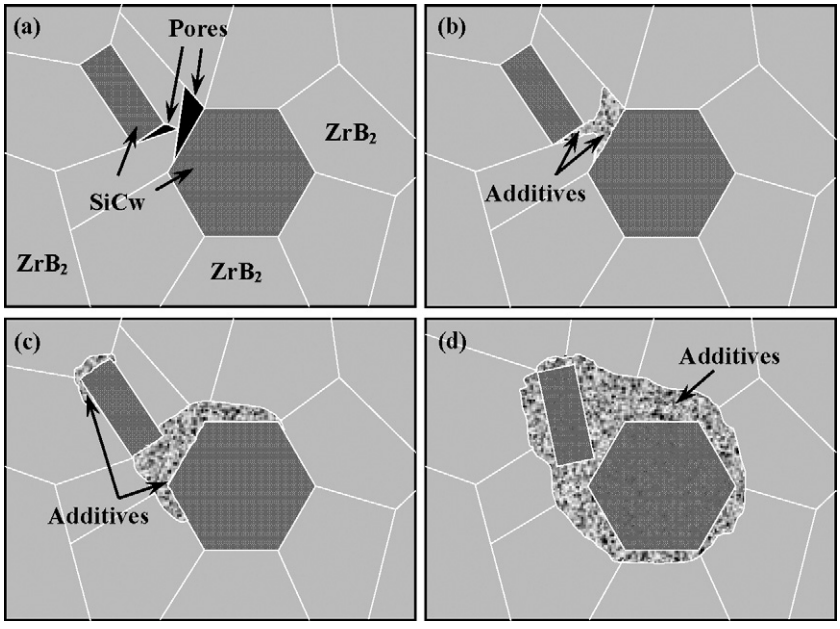

Fig. 7. Schematic illustration of the effect of different amount of additives on the microstructure of ZrB_2–SiCw composites, (a) 0, (b) 3, (c) 6, and (d) 10 vol.%.

anisms during sintering.[19,30] These two aspects make it difficult to densify ZrB_2–SiC composites and only 95% of relative density was obtained for pure ZrB_2–SiCw composite hot-pressed at 1800 °C for 60 min under a uniaxial load of 30 MPa in the present study. It is important to mention that ZrB_2–SiCw is more hard to sinter than ZrB_2–SiCp composite (SiCp denotes SiC particulate) with the same grain size and purity quotient of ZrB_2 powders due to the large size in length (>10 μm) of SiC whiskers. Thus, pores are observed in ZrB_2–SiCw composite without sintering additives, especially in the conjoint section of the ZrB_2 grains and SiC whiskers as shown in Figs. 3a and 7a.

On the contrary, ZW3AY, produced with the 3 vol.% sintering additives, revealed an earlier and faster shrinkage during hot-pressing and then reached higher relative density (Fig. 1). The presence of Al_2O_3 and Y_2O_3 promotes the formation of a transient liquid phase in ZrB_2–SiCw composite, similarly to the liquid sintering of SiC,[32] TiB_2[34] and ZrB_2.[23–26] At first, this liquid phase formed around ZrB_2 particles and SiC whiskers at high temperature, contributes to the glide and rearrangement of grains organization.[35] During this rearrangement process, liquid phase would react with surface oxide impurities of starting powders (i.e. B_2O_3, SiO_2, and ZrO_2). Meanwhile, little residual metallic impurities in raw powders such as Mg may also dissolves into liquid phase. From this point, additives act a "collector" at this stage. The similar "collection" function of liquid phase was also reported in ZrB_2–SiCp composites.[19] When the surface impurities were consumed completely, ZrB_2 grains and SiC whiskers became contact with the liquid phase. Surface atom or molecule diffusion was boosted with the help of liquid phase.[36] Meanwhile, the composition of the glass at grain boundary differ from that present in the interior. This composition gradient can lead to a normal traction in the surface of liquid phase and thus contribute to draw the liquid out of the boundaries.[36] This was also called "de-wetting" process. Wetting and de-wetting are determined by the competition of boundary energy between grain boundary and triple boundary.[37] During this process, liquid exudes to triple points and pores in hetero-phase conjoint sections, as shown in Figs. 4–7. Two kinds of grain boundaries were formed through these wetting and de-wetting processes. As shown in Fig. 8a, far from triple points, grains contacted directly, with interface clean and generally free of reaction products. However, a 6.5 nm width grain boundary was observed nearby the triple points filled with additives, can be seen in Fig. 8b.

As discussed above, it is generally believed that this temporary liquid phase would benefit the sintering and densification. Besides the effect on diffusion rate of atomic species, liquid phase can also promote the glide and rearrangement of grain organization, and more important it can plug into the porosities with the effect of de-wetting and capillary force. Thus, the relative density was higher than that of composite with no additives.

When the additives increasing to 6 or 10 vol.%, relative density showed no obvious increment (Fig. 1) and low-magnification SEM microstructure changed little as compared to that of composite with 3 vol.% additives (Fig. 3). However, under high-magnification SEM analysis, core-rim-like structures were obtained for both 6 and 10 vol.% adoption composites, as shown in Figs. 5 and 6. This suggests that similar de-wetting phenomenon was happened during sintering process and liquid was driven out grain boundaries. With the effect of rearrangement action from such redundant liquid phase, SiC whiskers were inclined to gather together and be enveloped by excessive liquids (Figs. 5–7). Therefore, relative densities of sintered composites didn't show distinct increase with additives increasing to 6 or 10 vol.%, as shown in Fig. 1.

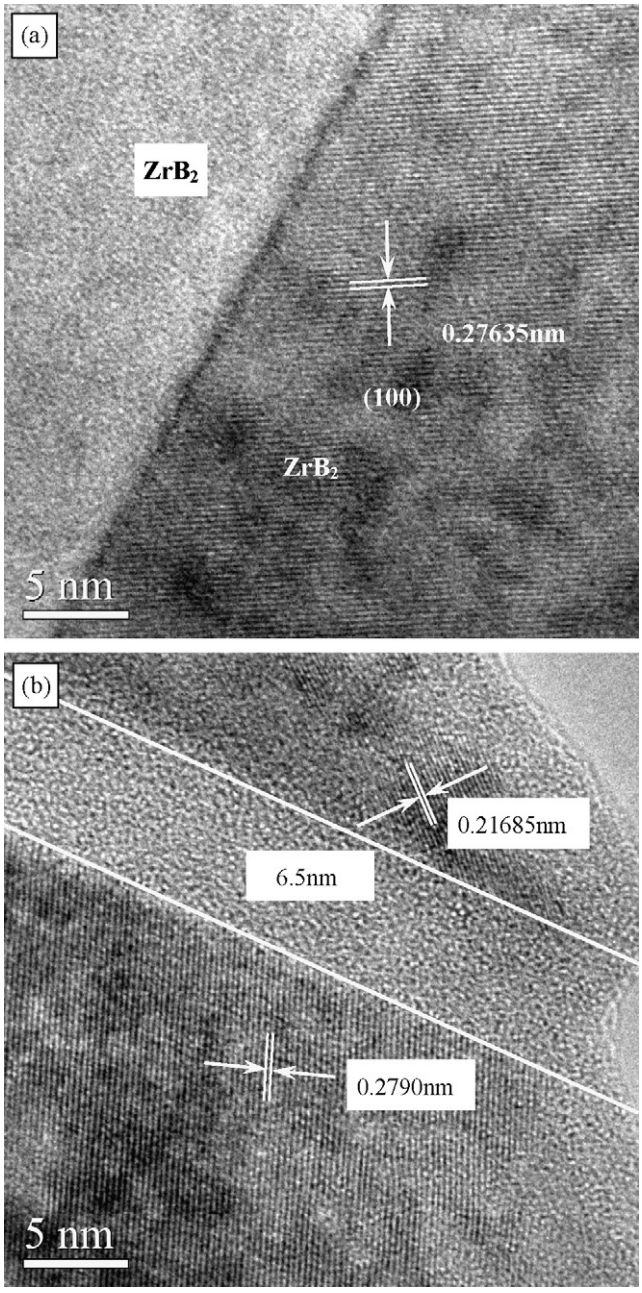

Fig. 8. HREM image of ZW3AY composite, showing two kinds of grain boundaries: far from (a) and near by (b) triple point.

3.3. Mechanical properties

Besides densification behavior and microstructure, the effects of additive amounts on mechanical properties were also studied.

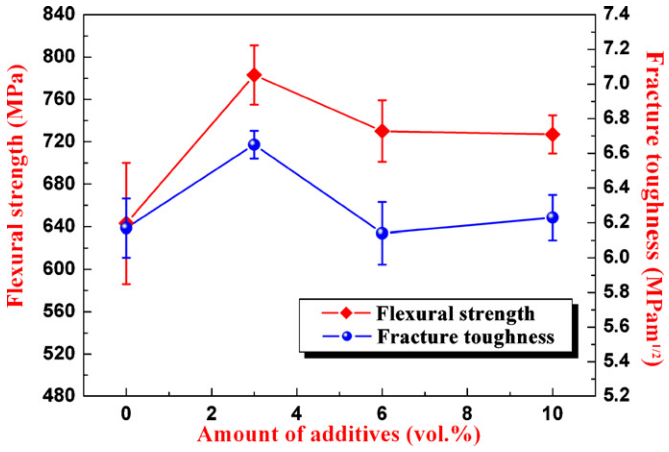

Fig. 9. Flexural strength and fracture toughness of ZrB_2–SiCw composites with different amounts of additives.

The room-temperature flexural strength and fracture toughness of four composites were plotted in Fig. 9. It indicates that the strength increases with the introduction of sintering additives. An addition of 3 vol.% additives increases the flexural strength from 643 MPa for the ZrB_2–SiCw composite with no additives to a maximum value of 783 MPa. This increase in strength was mainly attributed to the improvement of density and introduction of nano-size pocket phase (Figs. 1 and 2). However, the further increment of sintering additives decreases it to 730 MPa for 6 vol.% additives and 727 MPa for 10 vol.% additives. The flexural strength of sintered composites lies within the reported typical range of 650–850 MPa, as listed in Table 2.[19,29,38–40] The relative higher strength of ~1000 MPa could be a result of the finer starting powders and finer grains obtained in the final bulks.[39]

The fracture toughness of ZrB_2–SiCw composites at room temperature was also shown in Fig. 9. The variation of fracture toughness with additive content was similar to that of flexural strength. The fracture toughness values ranged from 6.1 to 6.7 MPa $m^{1/2}$, with the maximum value obtained for composite adopted with 3 vol.% additives. Fracture surfaces of the four different specimens were given in Fig. 10. It can be found that the fracture mode of pure ZrB_2–SiCw composite was transgranular, where the grain size was large and the fracture surface was flat. Meanwhile, porosities were found in the conjunction points of ZrB_2 grains and SiC whiskers. However, the roughness of fracture surface was increased and the fracture pattern of composites was changed to a mixed of intergranular/transgranular by the addition of 3 vol.% additives. This addition of small amount of additives also significantly increased the relative density and refined the grain size of the ZrB_2 grains, as shown in Fig. 10b. Thus, the flexural strength and fracture toughness appears to be improved with the adoption of additives. With the further increase of additives, it's interesting to note that the fracture mode recurred to prominent transgranular pattern and obvious coarsening was observed in ZrB_2 grains, especially for 10 vol.%. This was probably attributed to redundant liquid phase which was continuously embedded in the matrix of ZrB_2–SiCw composites. Similar phenomena have been reported in previous

Table 2
Relative density and mechanical properties of various ZrB_2-based matrix ceramic composites.

Composition	Rd (%)	K_{IC} (MPa $m^{1/2}$)	σ (MPa)	Ref.
ZrB_2–20SiCp	100	4.5	391	38
ZrB_2–20SiCp	99.7	4.4	1003	39
ZrB_2–20SiCp–3Y_2O_3	99.3	5.6	659	29
ZrB_2–20SiCp–5AlN	100	5.5	835	40
ZrB_2–20SiCp–4Si_3N_4	98	–	730	19
ZrB_2–20SiCw–3YAG	98.3	6.7	783	Present work

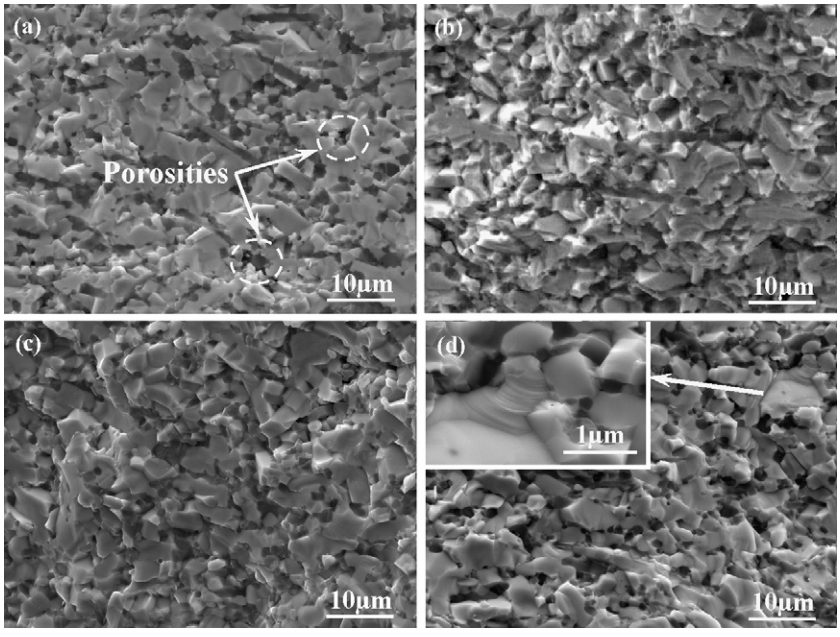

Fig. 10. Fracture surfaces of ZrB_2–SiCw composites with different additive contents: (a) 0, (b) 3, (c) 6, and (d) 10%.

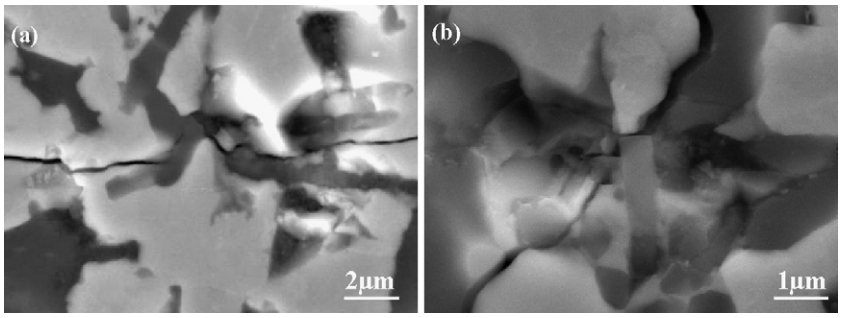

Fig. 11. SEM micrographs of indentation-induced crack propagation on a polished surface of ZW3AY: (a) crack deflection and whisker bridging and (b) whisker pull-out.

works for composites sintered with the addition of Y_2O_3[41] and YAG.[42]

Compared with the reported values (also shown in Table 2), the fracture toughness in this study was obvious higher due to the acicular-like SiC whiskers. To understand the toughening mechanisms of SiC whiskers, the specimens were indented using a load of 10 kg and the paths of indentation cracks were observed. As shown in Fig. 11 a and b, the crack deflection around whiskers, whisker bridging and pull-out were clearly observed during crack propagation process for the SiC whiskers reinforced ZrB_2 ceramic composite. It is believed that these interaction effects absorb crack propagation energy during fracture and lead to the improved toughness.[43]

4. Conclusions

ZrB_2–20 vol.%SiCw ultra-high temperature ceramics were produced by hot-pressing at a temperature of 1800 °C for 60 min. The effect of the sintering additives of Al_2O_3 plus Y_2O_3 on densification behavior, microstructure and mechanical properties was investigated. When a small amount of additives (3 vol.%) was added, the sinterability was improved significantly. The depletion of impurities (i.e. surface oxygen impurities and residual metallic impurities) and formation of transient liquid phase enhanced the sintering and densification. With this improvement in densification behavior, mechanical properties such as flexural strength and fracture toughness increased distinctively, as compared with those of composite with no addition. However, with further addition of additives ($\geq$6 vol.%), SiC whiskers were inclined to gather together and mechanical properties were not improved, due to the extensive formation of liquid phases in sintered composites. The flexural strength (783 MPa) was comparable to typical values for ZrB_2-based composites reinforced by SiC particles. Meanwhile, the fracture toughness (6.7 MPa $m^{1/2}$) was higher than previously reported values of ZrB_2–SiCp composites, due to the long aspect ratio of SiC whiskers.

Acknowledgements

This work was supported by the National Natural Science Foundation of China (50602010 and 90505015), the Research Fund for the Doctoral Program of Higher Education (20060213031) and the Program for New Century Excellent Talents in University.

References

1. Upadhya, K., Yang, J. M. and Hoffman, W. P., Materials for ultrahigh temperature structural applications. *Am. Ceram. Soc. Bull.*, 1997, **76**(12), 51–56.
2. Loehman, R., Corral, E., Dumm, H. P., Kotula, P. and Tandon, R., Ultra high temperature ceramics for hypersonic vehicle applications. *Sandia National Laboratories. Sandia report*, Sand 006-2925.
3. Kuriakose, A. K. and Margrave, J. L., The oxidation kinetics of zirconium diboride and zirconium carbide at high temperatures. *J. Electrochem. Soc.*, 1964, **111**(7), 827–831.
4. Tripp, W. C., Davis, H. H. and Graham, H. C., Effect of a SiC addition on the oxidation of ZrB_2. *Am. Ceram. Soc. Bull.*, 1973, **52**(8), 612–616.
5. Guo, S. Qi., Nishimura, T., Mizuguchi, T. and Kagawa, Y., Mechanical properties of hot-pressed ZrB_2–$MoSi_2$–SiC composites. *J. Eur. Ceram. Soc.*, 2008, **28**(9), 1891–1898.
6. Rezaie, A., Fahrenholtz, W. G. and Hilmas, G. E., Evolution of structure during the oxidation of zirconium diboride–silicon carbide in air up to 1500 °C. *J. Eur. Ceram. Soc.*, 2007, **27**(6), 2495–2501.
7. Monteverde, F. and Savino, R., Stability of ultra-high-temperature ZrB_2–SiC ceramics under simulated atmospheric re-entry conditions. *J. Eur. Ceram. Soc.*, 2007, **27**(16), 4797–4805.
8. Ghosh, D., Subhash, G., Radhakrishnan, R. and Sudarshan, T. S., Scratch-induced microplasticity and microcracking in zirconium diboride–silicon carbide composite. *Acta Mater.*, 2008, **56**(13), 3011–3022.
9. Passerone, A., Muolo, M. L., Valenza, F., Monteverde, F. and Sobczak, N., Wetting and interfacial phenomena in Ni–HfB_2 systems. *Acta Mater.*, 2009, **57**(2), 356–364.
10. Tang, S. F., Deng, J. Y., Wang, S. J. and Liu, W. C., Fabrication and characterization of an ultra-high-temperature carbon fiber-reinforced ZrB_2–SiC matrix composite. *J. Am. Ceram. Soc.*, 2007, **90**(10), 3320–3322.
11. Bartuli, C., Valente, T. and Tului, M., Plasma spray deposition and high temperature characterization of ZrB_2–SiC protective coatings. *Surf. Coat. Technol.*, 2002, **155**(2/3), 260–273.
12. Singh, M. and Asthana, R., Joining of zirconium diboride-based ultra high-temperature ceramic composites using metallic glass interlayers. *Mater. Sci. Eng. A*, 2007, **460/461**, 153–162.
13. Zhao, Y., Wang, L. J., Zhang, G. J., Jiang, W. and Chen, L. D., Preparation and microstructure of a ZrB_2–SiC composite fabricated by the spark plasma sintering-reactive synthesis (SPS-RS) method. *J. Am. Ceram. Soc.*, 2007, **90**(12), 4040–4042.
14. Wang, H. L., Wang, C. A., Yao, X. F. and Fang, D. N., Processing and mechanical properties of zirconium diboride-based ceramics prepared by spark plasma sintering. *J. Am. Ceram. Soc.*, 2007, **90**(7), 1992–1997.
15. Parthasarathy, T. A., Rapp, R. A., Opeka, M. and Kerans, R. J., A model for the oxidation of ZrB_2 HfB_2 and TiB_2. *Acta. Mater.*, 2007, **55**(17), 5999–6010.

16. Bongiorno, A., Forst, C. J., Kalia, R. K., Li, J., Marschall, J., Nakano, A. *et al.*, A perspective on modeling materials in extreme environments: oxidation of ultrahigh-temperature ceramics. *MRS Bull.*, 2006, **31**(5), 410–417.
17. Vajeeston, P., Ravindran, P., Ravi, C. and Asokamani1, R., Electronic structure, bonding, and ground-state properties of AlB_2-type transition-metal diborides. *Phys. Rev. B*, 2001, **63**(045115), 1–12.
18. Li, J., Lenosky, T. J., Forst, C. J. and Yip, S., Thermochemical and mechanical stabilities of the oxide scale of $ZrB_2 + SiC$ and oxygen transport mechanisms. *J. Am. Ceram. Soc.*, 2008, **91**(5), 1475–1480.
19. Monteverde, F., Guicciardi, S. and Bellosi, A., Advances in microstructure and mechanical properties of zirconium diboride based ceramics. *Mater. Sci. Eng. A*, 2003, **346**(1/2), 310–319.
20. Fahrenholtz, W. G., Hilmas, G. E., Talmy, I. G. and Zaykoski, J. A., Refractory diborides of zirconium and hafnium. *J. Am. Ceram. Soc.*, 2007, **90**(5), 1347–1364.
21. Kalish, D., Clougherty, E. V. and Kreder, K., Strength, fracture mode, and thermal stress resistance of HfB_2 and ZrB_2. *J. Am. Ceram. Soc.*, 1969, **52**(1), 30–36.
22. Kalish, D. and Clougherty, E. V., Densification mechanisms in high-pressure hot-pressing of HfB_2. *J. Am. Ceram. Soc.*, 1969, **52**(1), 26–30.
23. Meléndez-Martínez, J. J., Domínguez-Rodríguez, A., Monteverde, F., Melandri, C. and Portu, D. G., Characterisation and high temperature mechanical properties of zirconium boride-based materials. *J. Euro. Ceram. Soc.*, 2002, **22**(14/15), 2543–2549.
24. Venkateswaran, T., Basu, B., Raju, G. B. and Kim, D. Y., Densification and properties of transition metal borides-based cermets via spark plasma sintering. *J. Eur. Ceram. Soc.*, 2006, **26**(13), 2431–2440.
25. Mishra, S. K., Das, S. K., Ray, A. K. and Ramachandrarao, P., Effect of Fe and Cr addition on the sintering behavior of ZrB_2 produced by self-propagating high-temperature synthesis. *J. Am. Ceram. Soc.*, 2002, **85**(11), 2846–2848.
26. Monteverde, F. and Scatteia, L., Resistance to thermal shock and to oxidation of metal diborides–SiC ceramics for aerospace application. *J. Am. Ceram. Soc.*, 2007, **90**(4), 1130–1138.
27. Monteverde, F. and Bellosi, A., Beneficial effects of AlN as sintering aid on microstructure and mechanical properties of hot-pressed ZrB_2. *Adv. Eng. Mater.*, 2003, **5**(7), 508–512.
28. Guo, S. Q., Kagawa, Y. and Nishimura, T., Mechanical behavior of two-step hot-pressed ZrB_2-based composites with $ZrSi_2$. *J. Eur. Ceram. Soc.*, 2009, **29**(4), 787–794.
29. Zhang, X. H., Li, X. Y., Han, J. C., Han, W. B. and Hong, C. Q., Effects of Y_2O_3 on microstructure and mechanical properties of ZrB_2–SiC ceramics. *J. Alloys Compd.*, 2008, **465**(1/2), 506–511.
30. Zhang, S. C., Hilmas, G. E. and Fahrenholtz, W. G., Pressureless densification of zirconium diboride with boron carbide additions. *J. Am. Ceram. Soc.*, 2006, **89**(5), 1544–1550.
31. Zhu, S. M., Fahrenholtz, W. G., Hilmas, G. E. and Zhang, S. C., Pressureless sintering of carbon-coated zirconium diboride powders. *Mater. Sci. Eng. A*, 2007, **459**(1/2), 167–171.
32. Castillo-Rodríguez, M., Muñoz, A. and Domínguez-Rodríguez, A., Effect of atmosphere and sintering time on the microstructure and mechanical properties at high temperatures of α-SiC sintered with liquid phase Y_2O_3–Al_2O_3. *J. Eur. Ceram.*, 2006, **26**(12), 2397–2405.
33. Zhang, N., Ru, H. Q., Cai, Q. K. and Sun, X. D., The influence of the molar ratio of Al_2O_3 to Y_2O_3 on sintering behavior and the mechanical properties of a SiC–Al_2O_3–Y_2O_3 ceramic composite. *Mater. Sci. Eng. A*, 2008, **486**(1/2), 262–266.
34. Park, J. H., Koh, Y. H., Kim, H. E., Hwang, C. S. and Kang, E. S., Densification and mechanical properties of titanium diboride with silicon nitride as a sintering aid. *J. Am. Ceram. Soc.*, 1999, **82**(11), 3037–3042.
35. Kingery, W. D., Densification during sintering in the presence of a liquid phase. *J. Appl. Phys.*, 1959, **30**, 301–306.
36. Raj, R. and Chyung, C. R., Solution-precipitation creep in glass ceramics. *Acta Metall.*, 1981, **29**(1), 159–166.
37. Lewis, A. C., Josell, D. and Weihs, T. P., Stability in thin film multilayers and microlaminates: the role of free energy, structure, and orientation at interfaces and grain boundaries. *Scr. Mater.*, 2003, **48**(8), 1079–1085.
38. Levine, S. R., Opila, E. J., Halbig, M. C., Kiser, J. D., Singh, M. and Salem, J. A., Evaluation of ultra-high temperature ceramics for aeropropulsion use. *J. Eur. Ceram. Soc.*, 2002, **22**(14/15), 2757–2767.
39. Chamberlain, A. L., Fahrenholtz, W. G., Hilmas, G. E. and Ellerby, D. T., High-strength zirconium diboride-based ceramics. *J. Am. Ceram. Soc.*, 2004, **87**(6), 1170–1172.
40. Han, W. B., Li, G., Zhang, X. H. and Han, J. C., Effect of AlN as sintering aid on hot-pressed ZrB_2–SiC ceramic composite. *J. Alloys Compd.*, 2009, **471**(1/2), 488–491.
41. Suzuki, Y., Morgan, P. E. D. and Niihara, K., Improvement in mechanical properties of powder-processed $MoSi_2$ by the addition of Sc_2O_3 and Y_2O_3. *J. Am. Ceram. Soc.*, 1998, **81**(12), 3141–3149.
42. Ortiz, A. L., Muñoz-Bernabé, A., Borrero-López, O., Domínguez-Rodríguez, A., Guiberteau, F. and Padture, N. P., Effect of sintering atmosphere on the mechanical properties of liquid-phase-sintered SiC. *J. Eur. Ceram. Soc.*, 2004, **24**(10/11), 3245–3249.
43. Brennan, J. J. and Nutt, S. R., SiC-whisker-reinforced glass–ceramic composites: interfaces and properties. *J. Am. Ceram. Soc.*, 1992, **75**(5), 1205–1216.